



Article

Performance Assessment of Multi-GNSS PPP Ambiguity Resolution with LEO-Augmentation

Qin Li ¹, Wanqiang Yao ¹, Rui Tu ^{2,3,4,*}, Yanjun Du ¹ and Mingyue Liu ^{2,4}

- ¹ College of Geomatics, Xi'an University of Science and Technology, Xi'an 710054, China; 20110010005@stu.xust.edu.cn (Q.L.); duyanjun@stu.xust.edu.cn (Y.D.)
- ² National Time Service Center, Chinese Academy of Sciences, Shu Yuan Road, Xi'an 710600, China; liumingyue@ntsc.ac.cn
- ³ Key Laboratory of Precision Navigation and Timing Technology, Chinese Academy of Sciences, Shu Yuan Road, Xi'an 710600, China
- ⁴ University of Chinese Academy of Sciences, Yu Quan Road, Beijing 100049, China
- * Correspondence: turui-2004@126.com

Abstract: The fast motion of low Earth orbit (LEO) satellites provides rapid geometric changes in a short time, which can accelerate the initialization of precise point positioning (PPP). The rapid convergence of ambiguity parameters is conducive to the rapid success of ambiguity fixing. This paper presents the performance of single- and four-system combined PPP Ambiguity Resolution (AR), enhanced with an ambiguity-float solution LEO. Two LEO constellations were designed: L was a typical polar orbit constellation, with a higher number of visible satellites at high latitudes than at low and middle latitudes; and M was designed to compensate for the lack of visible satellites at low and middle latitudes. The ground observation data of the LEO satellites at the MGEX stations were simulated. Because the global navigation satellite systems (GNSSs) were fully operational, the GNSS data were real observation data from the MGEX stations. Based on the daily observation datasets collected at 258 stations in the global MGEX observation network over three days (from 1 January to 3 January 2022), in addition to the LEO simulation data, we evaluated the positioning performance of LEO ambiguity-float solution-enhanced PPP ambiguity resolution and compared it with LEO-enhanced PPP. The L+M mixed constellation was able to reduce the time to first fix (TTFF) of the four-system combined PPP-AR to 5 min, and four LEO satellites were sufficient to achieve this. L+M mixed constellation was able to reduce the convergence time of the four-system combined PPP to 2 min. Unlike PPP-AR, PPP required more LEO satellites for augmentation to saturate.

Keywords: low Earth orbit satellite; global navigation satellite system; precise point positioning; ambiguity resolution; convergence speed



Citation: Li, Q.; Yao, W.; Tu, R.; Du, Y.; Liu, M. Performance Assessment of Multi-GNSS PPP Ambiguity Resolution with LEO-Augmentation. *Remote Sens.* **2023**, *15*, 2958. <https://doi.org/10.3390/rs15122958>

Academic Editor: Michael E. Gorbunov

Received: 20 May 2023

Revised: 31 May 2023

Accepted: 5 June 2023

Published: 6 June 2023



Copyright: © 2023 by the authors. Licensee MDPI, Basel, Switzerland. This article is an open access article distributed under the terms and conditions of the Creative Commons Attribution (CC BY) license (<https://creativecommons.org/licenses/by/4.0/>).

1. Introduction

Precise point positioning (PPP) [1] technology has been widely used in many fields, such as precision agriculture, precise mapping, deformation monitoring, water vapor inversion, precise navigation, and positioning [2], owing to its high positioning accuracy, simple structure, and flexible operation (without any reference station). However, it usually takes tens of minutes to achieve centimeter-level positioning accuracy. Reliable ambiguity resolution (AR) [3,4] also requires a longer observation time, due to the obstacle of atmospheric errors, especially ionospheric delays. Regional augmentation precise point positioning, also known as precise point and real time kinematic positioning (PPP-RTK) [5], utilizes precise atmospheric corrections (generated using the reference network) to accelerate ambiguity resolution [6]. Unfortunately, there are places where reference stations cannot be established or available, such as in oceans, deserts, or developing areas.

Many efforts have been made to improve PPP performance in terms of observations, such as combining multiple global navigation satellite systems (GNSSs) and using multife-

quency signals. GPS/GLONASS combined PPP can improve the convergence speed [7], but the positioning accuracy is not as good as the GPS-only PPP when the orbit and clock offset quality of the GLONASS satellite is poor [8]. At the same time, GPS/GLONASS combined PPP can also accelerate the convergence of ambiguity parameters, thereby shortening the time to first fix (TTFF) of ambiguity [9,10]. For GPS/BDS/GLONASS/Galileo four-system combined PPP, compared with single-system PPP, multisystem combined positioning not only converges faster but also improves the availability of PPP technology in special environments, as well as the reliability of positioning results [11–13]. In addition to multisystem fusion, multifrequency observations can improve the performance of PPP. Based on simulated GPS three-frequency data, Geng et al. [14] conducted PPP fixed-solution experiments and pointed out that three-frequency PPP could achieve ambiguity-fixed solutions in a few minutes. Elsobeiey et al. [15] conducted PPP float solution experiments based on real GPS three-frequency data, and the results showed that the convergence time of three-frequency PPP could be shortened by 10%. Li et al. [16] found that the convergence speed and positioning accuracy of three-frequency PPP ambiguity resolution was better than that of three-frequency PPP and dual-frequency PPP-AR in the initialization stage, through a BDS three-frequency uncombined PPP-AR experiment. Li et al. [17] evaluated the performance of a BDS/Galileo combination with three-frequency PPP-AR, and the results showed that multi-GNSS fusion could further improve the position estimation capability of a single system. Not only were the observations themselves found to be beneficial for reducing the convergence time in PPP, but so too was the incorporation of external ionospheric corrections from multiscale network configurations [18,19]. However, due to the slow geometric change in the satellites' position relative to the ground station, PPP initialization still took approximately 10 min.

In addition to multi-GNSS and multifrequency satellites, low Earth orbit (LEO) satellites are another way to improve PPP performance. In recent years, commercial companies have proposed their own LEO constellation, consisting of hundreds to thousands of LEO satellites that would provide broadband Internet services worldwide. Reid et al. [20] demonstrated the potential of the LEO constellation as a navigation system, which was also confirmed in the first generation of the Iridium constellation. This constellation was the first low Earth orbit satellite constellation to integrate communication and navigation functions. It comprises 66 satellites distributed in six orbital planes, with an orbital altitude of 781 km and an orbital inclination of 86.4°. Compared with the ordinary GNSS medium-Earth orbit (MEO) satellite, the LEO constellation has the following advantages: First, the LEO satellite has a lower orbital height, being 20 times closer to Earth than the MEO satellite, in addition to a shorter signal transmission path, and a smaller degree of power loss. Therefore, the signal power received on the ground is stronger, and the anti-interference and anti-deception performance is better. For example, the signal power of the Iridium satellite is 1000 times that of GPS [21]. Therefore, even in highly shielded environments (such as indoors, in forests, under bridges, and inside canyons), users can still receive continuous LEO navigation signals. Second, the LEO satellite moves faster than the ground station, and the continuous observation duration is only 10–20 min. The Doppler frequency shift phenomenon is evident, which is favorable for the carrier phase cycle slip detection [22]. At the same time, the fast motion of LEO satellites provides rapid geometric changes in a short period of time, which can accelerate the initialization of PPP, thus shortening the convergence time of precise point positioning.

To prove the contribution of LEO to PPP, many researchers have conducted numerous LEO-enhanced precision point positioning experiments based on simulated observations. Ke et al. [23] tested the performance of LEO-enhanced GPS PPP and compared it with that of GPS or GPS/GLONASS combination schemes. The results showed that the convergence time of the LEO-enhanced GPS and GPS/GLONASS combined scheme was reduced by 51.31% and 3.93%, respectively, compared with the GPS-only scheme, indicating that the contribution of the LEO satellite to the convergence speed of the PPP was greater than that of a MEO satellite. Ge et al. [24] found that LEO-enhanced GNSSs

(GPS/BDS/Galileo) could reduce the convergence time of PPP to 5 min. Li et al. [25] studied the performance of LEO-enhanced GNSSs (GPS/GLONASS/BDS/Galileo) under LEO constellations with different satellite numbers (60, 96, 192, 288), orbital heights (1000 km, 600 km), and orbital types (polar orbit, sun-synchronous orbit), and proposed a LEO constellation scheme consisting of 192 satellites with an orbital altitude of 1000 km, which could significantly shorten the convergence time of GRCE PPP by more than 70%. Li et al. [26] analyzed the performance of PPP ambiguity resolution with LEO-augmented multi-GNSS (GPS/GLONASS/BDS/Galileo), and the results showed that with the enhancement of 60, 192, and 288 LEO constellations, the TTFF of GREC PPP-AR was shortened from 7.1 min to 4.8 min, 1.1 min, and 0.7 min, respectively, and the positioning accuracy was improved by approximately 60%, 80%, and 90%, respectively. The performance of the three-frequency LEO-enhanced PPP-AR was better than that of dual-frequency. Zhao et al. [27] found that in harsh environments, the float solution and fixed solution performance of triple-frequency uncombined BDS/GPS/LEO PPP were improved to different degrees compared with that of only BDS, which they ascertained through six sets of shielding experiments using different elevation and azimuth angles.

The above studies show that the LEO constellation can significantly improve the performance of PPP and PPP-AR; however, few studies have examined the contribution of the LEO float solution to PPP-AR. As mentioned above, the fast motion of LEO satellites provides rapid geometric changes in a short time, which can accelerate the initialization of PPP, and the fast convergence of ambiguity parameters is conducive to the rapid success of ambiguity fixing. Therefore, this study focused on the performance of the LEO float solution to enhance PPP-AR. The remainder of this article is structured as follows: The two LEO constellations we designed and the LEO observation simulation on the Multi-GNSS Experiment (MGEX) stations are introduced in Section 2. Because GNSSs (GPS/GLONASS/BDS-3/Galileo) were fully operational, the GNSS data are real observation data from MGEX stations. The functional model of LEO-enhanced GNSSs PPP and PPP-AR is introduced in Section 3. In Section 4, we introduce the positioning performance of single-system and the four-system combined PPP-AR enhanced using the LEO ambiguity-float solution, and then compare it with LEO-enhanced PPP. A summary of our results is presented in Section 5.

2. LEO Constellation Design and Ground Observation Simulation

In this study, two LEO constellations were designed: L and M, both of which were Walker constellations [28]. L consisted of 70 satellites distributed in six orbital planes, with an orbital altitude of 1000 km and an orbital inclination of 90° . M consisted of 90 satellites distributed in 10 orbital planes, with an orbital altitude of 1000 km and an orbital inclination of 60° . The main difference between the two LEO constellations was their orbital inclinations. Figure 1 shows the daily average number of visible satellites of the LEO constellation on 1 January 2022, at a cutoff elevation angle of 7° , with L, M, and L+M from top to bottom. The number of visible satellites from the L constellation in high latitudes was much greater than that in middle and low latitudes, because the L constellation is a polar orbit constellation with an inclination of 90° . The M constellation compensated for the lack of visible satellites in the low and middle latitudes of the L constellation, but it had no coverage in the polar regions, which was also caused by orbital inclination.

This study conducted LEO ground-observation simulations for all stations in the MGEX observation network. The simulation data included two frequencies, L1 (1575.42 MHz) and L2 (1227.60 MHz). Errors, such as satellite clock offsets, receiver clock offsets, relativistic effect, phase wind-up, tides, satellite and receiver antenna phase center offsets and variations, tropospheric delay, Earth rotation, and measurement noise, were considered. The dry and wet components of the tropospheric delay in the zenith direction were calculated using the Saastamoinen model [29], and the GMF projection function [30] was used to calculate the total tropospheric delay in the signal propagation direction. The measurement noise of the pseudorange and the carrier phase were 0.5 and 0.003 m, respectively.

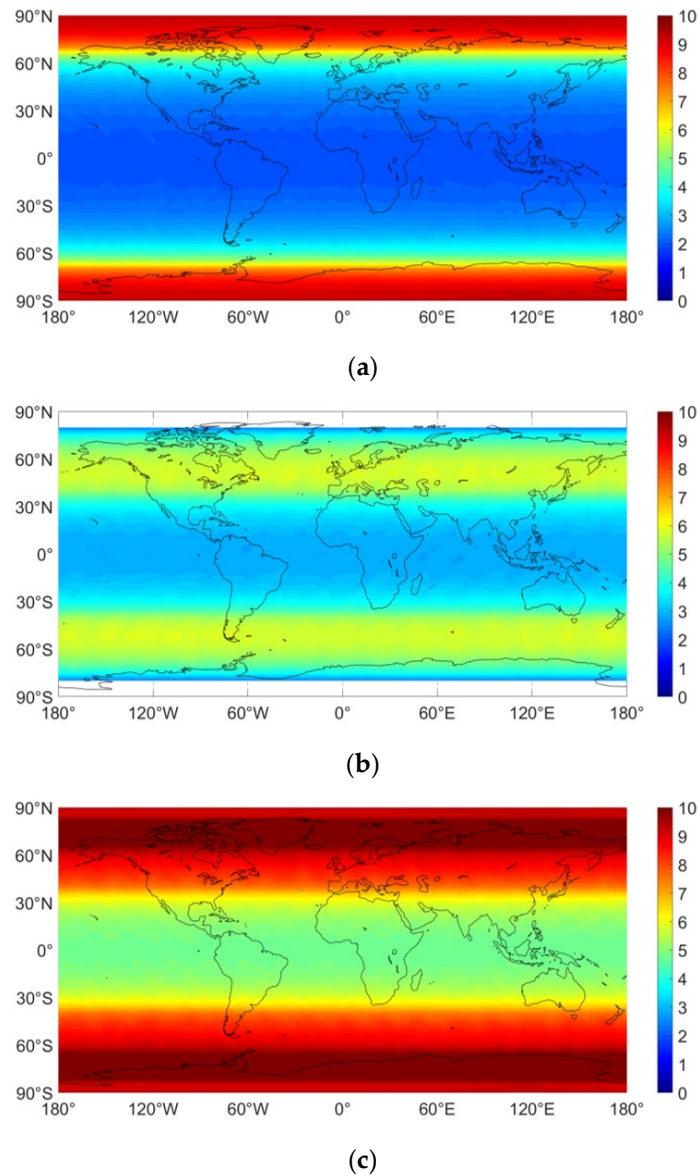


Figure 1. The daily average number of visible satellites in the LEO constellation on 1 January 2022. Different colors in the color bar represent different numbers of visible satellites: (a) L; (b) M; (c) L+M.

3. Methods

3.1. LEO-Enhanced GNSSs PPP

The observation of GNSSs PPP mainly included code pseudorange $P_{r,j}^{s,K}$ and carrier phase $L_{r,j}^{s,K}$, and its observation equation was expressed as follows:

$$P_{r,j}^{s,K} = \rho_r^{s,K} + c(dt_r - dt^{s,K}) + T_r^{s,K} + I_{r,j}^{s,K} + b_{r,j}^K - b_j^{s,K} + \varepsilon_{P_{r,j}^{s,K}}, \quad (1)$$

$$L_{r,j}^{s,K} = \rho_r^{s,K} + c(dt_r - dt^{s,K}) + T_r^{s,K} - I_{r,j}^{s,K} + \lambda_j^{s,K} (N_{r,j}^{s,K} + B_{r,j}^K - B_j^{s,K}) + \varepsilon_{L_{r,j}^{s,K}}, \quad (2)$$

where the subscript r is the station number, j represents the frequency point, the superscript s is the satellite number, and K represents GPS, GLONASS, BDS-3, or Galileo. $\rho_r^{s,K}$ indicates the geometric distance between the station and satellite. c is the speed of light in a vacuum, dt_r is the receiver clock offset, and $dt^{s,K}$ is the satellite clock offset. $T_r^{s,K}$ is the tropospheric delay and $I_{r,j}^{s,K}$ is the ionospheric delay at the frequency point j . $b_{r,j}^K$ and $b_j^{s,K}$ are the

code hardware delays at the receiver and satellite ends, respectively. $B_{r,j}^K$ and $B_j^{s,K}$ are the phase hardware delays at the receiver and satellite ends, respectively. $N_{r,j}^{s,K}$ is the integer ambiguity at the frequency point j . The corresponding wavelengths $\lambda_j^{s,K}$. $\varepsilon_{P_{r,j}^{s,K}}$ and $\varepsilon_{L_{r,j}^{s,K}}$ are the measurement noise errors of the code pseudorange and carrier phase, respectively. There were also some potential error items, such as Earth rotation, satellite and receiver antenna phase center variations and offsets, antenna wind up, solid tide, ocean tide, atmospheric tide, and relativistic effect, which were corrected according to existing models [31]; therefore, they have not been listed in the above equation.

To eliminate the first-order ionospheric delay of the code pseudorange and carrier phase observation, the ionospheric-free (IF) combination of $P_{r,IF}^{s,K}$ and $L_{r,IF}^{s,K}$ is usually used to estimate PPP parameters, and the combination mode of IF is

$$P_{r,IF}^{s,K} = \frac{(f_1^{s,K})^2}{(f_1^{s,K})^2 - (f_2^{s,K})^2} P_{r,1}^{s,K} - \frac{(f_2^{s,K})^2}{(f_1^{s,K})^2 - (f_2^{s,K})^2} P_{r,2}^{s,K}, \tag{3}$$

$$L_{r,IF}^{s,K} = \frac{(f_1^{s,K})^2}{(f_1^{s,K})^2 - (f_2^{s,K})^2} L_{r,1}^{s,K} - \frac{(f_2^{s,K})^2}{(f_1^{s,K})^2 - (f_2^{s,K})^2} L_{r,2}^{s,K}, \tag{4}$$

where $f_1^{s,K}$ and $f_2^{s,K}$ denote the different frequency points. In this study, GPS used L1 and L2, GLONASS used G1 and G2, BDS-3 used B1 and B3, and Galileo used E1 and E5a, which was consistent with the International GNSS Service (IGS) analysis center. The observation equation after the combination is

$$\begin{cases} P_{r,IF}^{s,K} = \rho_r^{s,K} + c(dt_r - dt^{s,K}) + T_r^{s,K} + b_{r,IF}^K - b_{IF}^{s,K} + \varepsilon_{P_{r,IF}^{s,K}} \\ L_{r,IF}^{s,K} = \rho_r^{s,K} + c(dt_r - dt^{s,K}) + T_r^{s,K} + \lambda_{IF}^{s,K}(N_{r,IF}^{s,K} + B_{r,IF}^K - B_{IF}^{s,K}) + \varepsilon_{L_{r,IF}^{s,K}} \end{cases}, \tag{5}$$

where $b_{r,IF}^K$ and $b_{IF}^{s,K}$ are the code hardware delays of the IF combination at the receiver and satellite ends, respectively. For frequency division multiple access systems, such as GLONASS, $b_{r,IF}^K$ represents the average hardware delay at the receiver end. $B_{r,IF}^K$ and $B_{IF}^{s,K}$ are the phase hardware delays of the ionospheric-free combination at the receiver and satellite ends, respectively. $\lambda_{IF}^{s,K}$ and $N_{r,IF}^{s,K}$ are the carrier wavelength and ambiguity of the IF combination, respectively. $\varepsilon_{P_{r,IF}^{s,K}}$ and $\varepsilon_{L_{r,IF}^{s,K}}$ are the measurement noise error of the code pseudorange and the carrier phase of the IF combination, respectively. The ambiguity, code, and phase hardware delays of the IF combination are as follows.

$$b_{r,IF}^K = \left((f_1^{s,K})^2 b_{r,1}^K - (f_2^{s,K})^2 b_{r,2}^K \right) / \left((f_1^{s,K})^2 - (f_2^{s,K})^2 \right), \tag{6}$$

$$b_{IF}^{s,K} = \left((f_1^{s,K})^2 b_1^{s,K} - (f_2^{s,K})^2 b_2^{s,K} \right) / \left((f_1^{s,K})^2 - (f_2^{s,K})^2 \right), \tag{7}$$

$$B_{r,IF}^K = c \left(f_1^{s,K} B_{r,1}^K - f_2^{s,K} B_{r,2}^K \right) / \lambda_{IF}^{s,K} \left((f_1^{s,K})^2 - (f_2^{s,K})^2 \right), \tag{8}$$

$$B_{IF}^{s,K} = c \left(f_1^{s,K} B_1^{s,K} - f_2^{s,K} B_2^{s,K} \right) / \lambda_{IF}^{s,K} \left((f_1^{s,K})^2 - (f_2^{s,K})^2 \right), \tag{9}$$

$$N_{r,IF}^{s,K} = c \left(f_1^{s,K} N_{r,1}^{s,K} - f_2^{s,K} N_{r,2}^{s,K} \right) / \lambda_{IF}^{s,K} \left((f_1^{s,K})^2 - (f_2^{s,K})^2 \right), \tag{10}$$

To reduce satellite orbit and clock errors, precision ephemeris and precision satellite clock products are generally used in PPP. Because the precision satellite clock error is generated from the IF combined pseudorange observation data of the GNSS ground tracking network, the $dt^{s,K}$ provided by the IGS absorbed the code hardware delay $b_{IF}^{s,K}/c$ of the IF combination at the satellite end. The code hardware delay at the receiver end varied

with different satellite systems (such a difference is called intersystem bias), and it will be absorbed by the receiver clock error; therefore, the receiver-clock offsets of different satellite systems are different. The ambiguity parameter is closely related to the phase hardware delay. They all have constant characteristics, which vary between different satellites, making it difficult to separate them from each other. Simultaneously, owing to the introduction of the satellite clock error based on pseudorange observation, the code hardware delay at the satellite end was introduced into the phase observation equation, being then absorbed by the ambiguity parameter. Because the pseudorange observation equation and phase observation equation work together to estimate the receiver clock error, the code hardware delay at the receiver end was also introduced into the phase observation equation and absorbed by the ambiguity parameter. Therefore, because the satellite clock error was corrected by the precise product, Equation (5) could be rewritten as

$$\begin{cases} P_{r,IF}^{s,K} = \rho_r^{s,K} + \bar{c}dt_r^K + T_r^{s,K} + \varepsilon_{P_{r,IF}^{s,K}} \\ L_{r,IF}^{s,K} = \rho_r^{s,K} + \bar{c}dt_r^K + T_r^{s,K} + \lambda_{IF}^{s,K} \bar{N}_{r,IF}^{s,K} + \varepsilon_{L_{r,IF}^{s,K}} \end{cases}, \quad (11)$$

where the reparameterized receiver clock error and ambiguity are shown in Equations (12)–(15). In addition, the three-dimensional position of the receiver and the tropospheric wet delay in the zenith direction have been estimated:

$$\bar{c}dt_r^K = cdt_r + b_{r,IF}^K, \quad (12)$$

$$\bar{N}_{r,IF}^{s,K} = N_{r,IF}^{s,K} + d_{r,IF}^K - d_{IF}^{s,K}, \quad (13)$$

$$d_{r,IF}^K = B_{r,IF}^K - b_{r,IF}^K / \lambda_{IF}^{s,K}, \quad (14)$$

$$d_{IF}^{s,K} = B_{IF}^{s,K} - b_{IF}^{s,K} / \lambda_{IF}^{s,K}, \quad (15)$$

where $d_{r,IF}^K$ is the receiver uncalibrated phase delay (UPD), and $d_{IF}^{s,K}$ is the satellite UPD. As seen in the above formula, the IF combined ambiguity parameter $\bar{N}_{r,IF}^{s,K}$ contains the hardware delay of the receiver and satellite and loses the integer characteristic. However, it cannot be separated directly with single-station positioning. Usually, the two are combined for estimation, and the float solution is used.

Comprehensively, considering the error source of the LEO simulation data, the observation equation of LEO-enhanced GNSSs PPP is as follows:

$$\begin{cases} P_{r,IF}^{s,K} = \rho_r^{s,K} + \bar{c}dt_r^K + T_r^{s,K} + \varepsilon_{P_{r,IF}^{s,K}} \\ L_{r,IF}^{s,K} = \rho_r^{s,K} + \bar{c}dt_r^K + T_r^{s,K} + \lambda_{IF}^{s,K} \bar{N}_{r,IF}^{s,K} + \varepsilon_{L_{r,IF}^{s,K}} \\ P_{r,IF}^{s,L} = \rho_r^{s,L} + \bar{c}dt_r^L + \varepsilon_{P_{r,IF}^{s,L}} \\ L_{r,IF}^{s,L} = \rho_r^{s,L} + \bar{c}dt_r^L + \lambda_{IF}^{s,L} \bar{N}_{r,IF}^{s,L} + \varepsilon_{L_{r,IF}^{s,L}} \end{cases}, \quad (16)$$

In the formula, the superscript L represents the LEO system. The state vector of unknowns is $\vec{X} = [x \ y \ z \ \bar{d}t_r^K \ \bar{d}t_r^L \ ZWD \ \bar{N}_{r,IF}^{s,K} \ \bar{N}_{r,IF}^{s,L}]^T$, which will be estimated using a Kalman filter approach. Because the tropospheric dry and wet delays of the LEO simulation data are calculated using the Saastamoinen model (see Section 2), the LEO system does not need to estimate the tropospheric delay parameters, but instead directly uses the model to correct them. A stochastic model based on elevation angle [32] has been adopted, and the cut-off elevation angle was 7 degrees.

In the above formula, the narrow-lane FCB absorbs the wide-lane FCB. Narrow-lane FCBs can be obtained using an estimation process similar to that of wide-lane FCBs.

After accurate estimation of WL and NL FCBs, PPP-AR can be realized. According to Equation (20), the IF combination ambiguity is reversed, and the intersatellite single difference is used to eliminate the narrow-lane FCB at the receiver end to obtain Equation (21).

$$N_{\text{IF}}^{s,t} = \frac{f_1}{f_1 + f_2} \left(\tilde{N}_{\text{NL}}^{s,t} + \bar{f}_{\text{NL}}^{s,t} \right) + \frac{f_1 f_2}{f_1^2 - f_2^2} \tilde{N}_{\text{WL}}^{s,t}. \quad (21)$$

The LAMBDA search method was used to fix the integer ambiguity of the narrow-lane $\bar{f}_{\text{NL}}^{s,t}$, and the ratio value was set to 2. Taking the above equation as the constraint of the IF combined observation equation, the ambiguity-fixed solution of the PPP is calculated.

4. Analysis

To analyze the performance of the LEO float solution to enhance PPP-AR, observation data of 258 stations in the MGEX observation network from January 1 to 3, 2022 were selected, as shown in Figure 2. The experiments of single-system and four-system combined PPP-AR enhanced using LEO ambiguity-float solution were carried out for these stations and compared with LEO-enhanced PPP. The detailed data processing strategy is shown in Table 1. In Figure 2, the red dots indicate that we conducted LEO-enhanced GPS PPP and PPP-AR experiments on this site, the green dots indicate that we conducted LEO-enhanced Galileo PPP and PPP-AR experiments on this site, the blue dots indicate that we conducted LEO-enhanced GLONASS PPP experiments on this site, and the yellow dots indicate that we conducted LEO-enhanced BDS-3 PPP experiments on the site. The presence of four colors in one dot indicates that we carried out LEO-enhanced four-system combination PPP and PPP-AR experiments on the site. In all experiments, the reference coordinates of the experimental results were the coordinate values in the SNX weekly solution file provided by the IGS. Supplementary information, such as the precise satellite orbit and the clocks (post-processed products), were provided by the IGS data center of the German Research Centre for Geosciences.

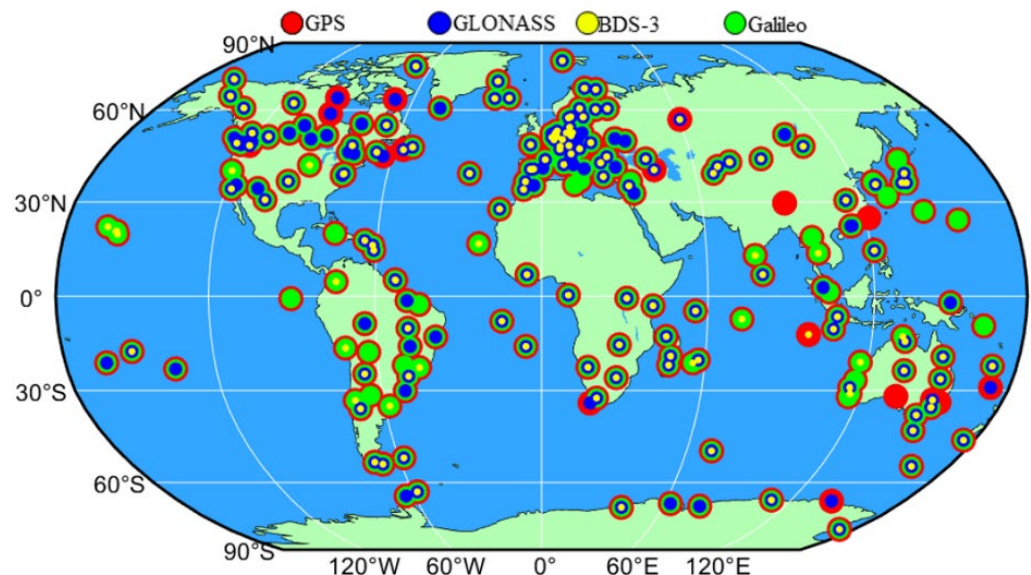


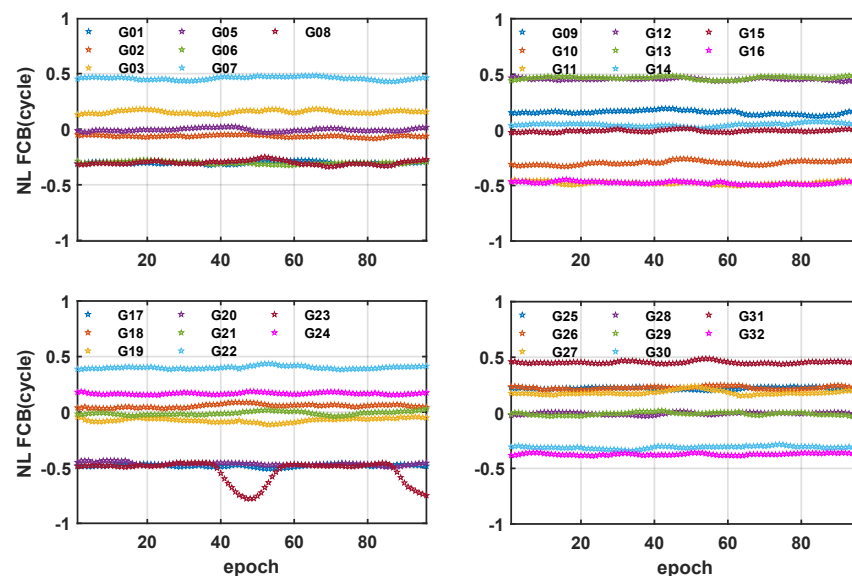
Figure 2. The distribution of MGEX stations: GPS (red); GLONASS (blue); BDS-3 (yellow); and Galileo (green).

Table 1. The detailed data processing strategy.

Items	Data Processing Strategy
Frequency	GPS/LEO: L1/L2; BDS-3: B1/B3;
Sampling	Galileo: E1/E5a; GLONASS: G1/G2
Observations	30 s
Cut-off elevation angle	IF observations of carrier phase and code pseudorange
Ambiguities	Float: 7°; Fix: 10°
Receiver coordinates	LEO/GLONASS: constant estimation
Receiver clock offsets	GPS/BDS-3/Galileo: constant estimation and ambiguities fixed
Tropospheric dry delay	Estimated as white noise
Tropospheric wet delay in the zenith direction	Saastamoinen model + GMF projection function
Ionospheric delay	LEO: Saastamoinen model correction
Satellite orbit and clock	GPS/GLONASS/BDS-3/Galileo: estimated by random walk
Satellite and receiver antenna phase center, and other modellable errors	Eliminated by IF observations Precise products Model correction

4.1. Quality of FCB Products

We used observation data from 152 globally distributed MGEX stations to estimate GCE FCBs, in addition to evaluating the daily stability of NL FCBs, as shown in Figure 3. NL FCBs in Galileo were the most stable, with all NL FCBs remaining within 0.1 cycles in a day. Among GPS satellites, the G23 satellite showed a range of 0.3 cycles, while other satellites remained stable within 0.1 cycles. For BDS-3, the stability was relatively poor. Satellites C34 and C46 had the largest changes, up to 0.6 cycles, while other satellites had changes within 0.4 cycles. Overall, BDS-3 exhibited the worst NL FCB stability among the three systems. The average STD of the NL FCBs for G, C, and E were 0.016, 0.054, and 0.014 cycles, respectively.



(a)

Figure 3. Cont.

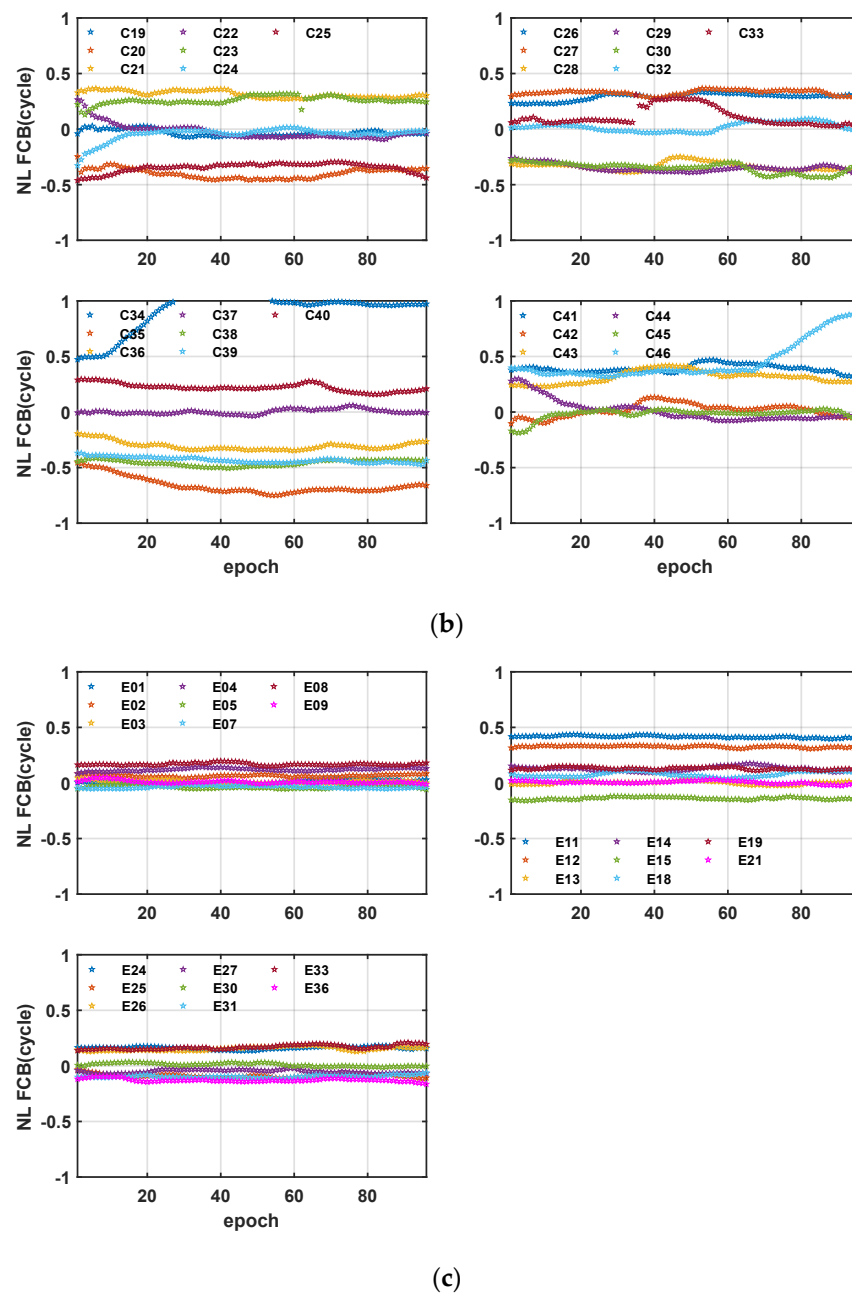


Figure 3. Time series of the NL GCE FCBs on 1 January 2022: (a) GPS; (b) BDS-3; and (c) Galileo.

4.2. LEO-Enhanced PPP and PPP-AR

4.2.1. PPP and PPP-AR Enhanced with Different LEO Constellations

The positioning performance of both PPP and PPP-AR (enhanced using the L, M, and L+M constellations) was evaluated using ground observation simulation data of different LEO constellations. MGEX station ASCG (7.92°S, 14.33°W) was selected as a typical example. The results of the single-system and four-system combined float solution, in addition to the fixed-solution PPP enhanced using different LEO constellations, for this station on 3 January 2022, are shown in Figure 4a,b. It can be seen that the addition of the LEO satellite could significantly accelerate the convergence of PPP, and effectively accelerated the first fix of PPP-AR. The convergence speeds in the east (E), north (N), and up (U) directions were clearly improved, and the fixed solutions exhibited similar results. Compared with single-system PPP, four-system combined PPP converges faster, leaving less room for improvement of LEO satellites. Similarly, the improvement of the fixed

solution was not as significant as that of the float solution. The L+M mixed constellation was the best, followed by the M constellation, and then the L constellation.

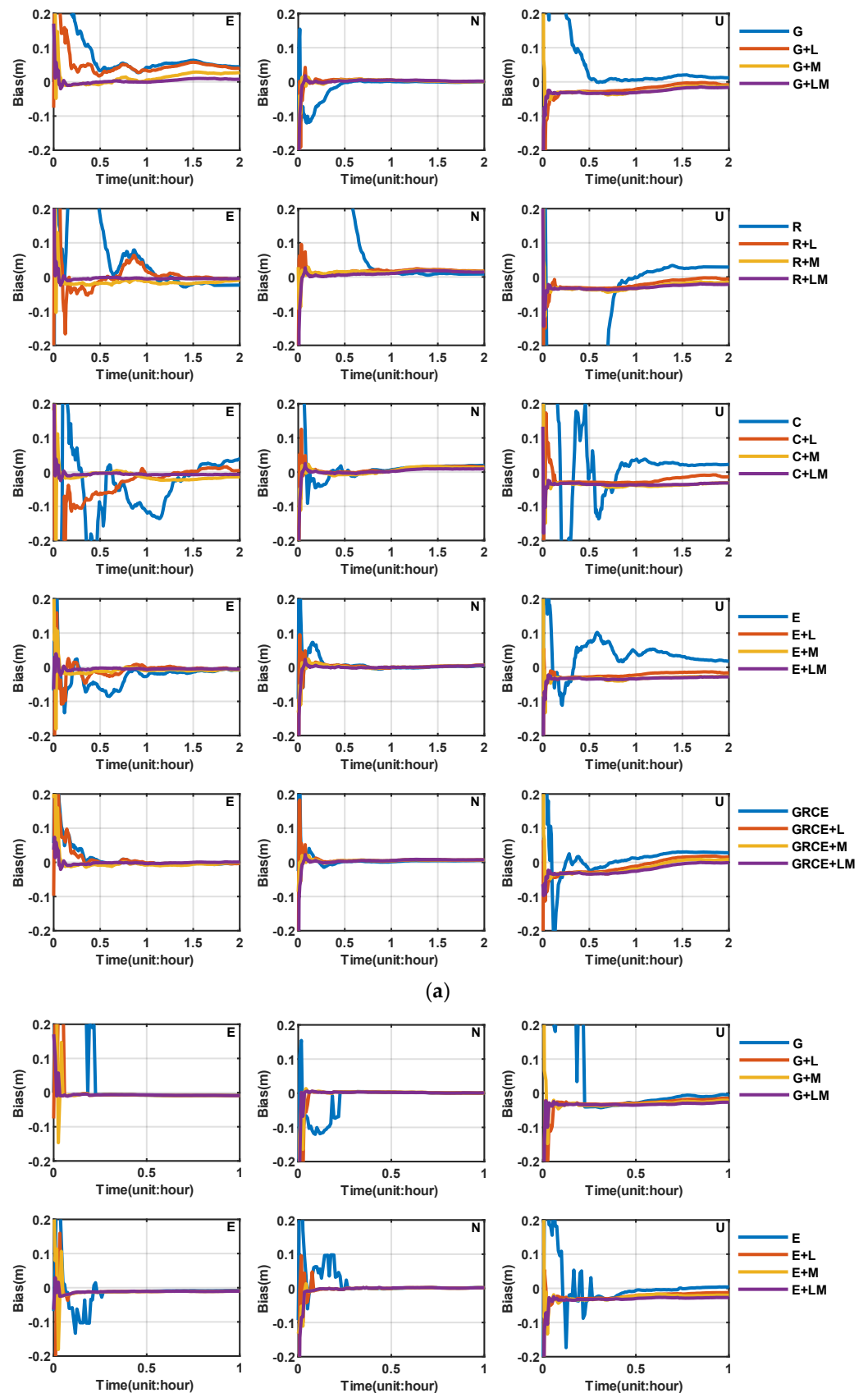


Figure 4. Cont.

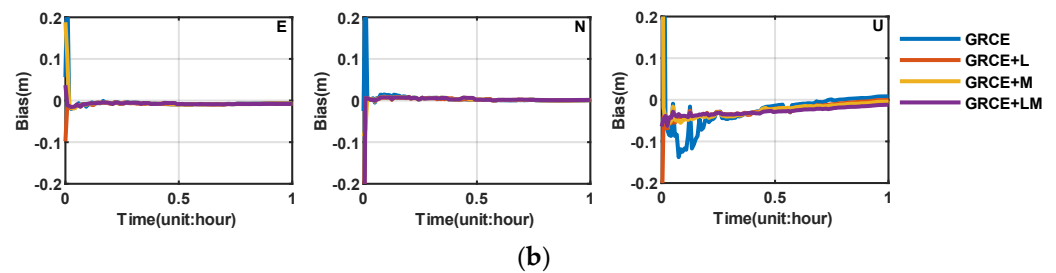


Figure 4. Comparison of positioning performances of different LEO constellations augmented PPP and PPP-AR in east, north, and up directions, respectively, at station ASCG on 3 January 2022: (a) PPP; (b) PPP-AR.

Figure 5 shows the average convergence time of PPP enhanced using different LEO constellations. In this study, the convergence time was set as the time when the positioning error in the E, N, and U directions was less than 0.1 m and lasted for 10 min. By introducing the L, M, and L+M constellations, the convergence time of single-system PPP was shortened from 29.1 to 9.7, 5.7, and 2.3 min, and the convergence time of the four-system combined PPP could be shortened from 11.4 to 6.1, 3.0, and 1.8 min. The L+M constellation showed the shortest times, followed by the M constellation, and then the L constellation. This was because the L constellation had few visible satellites in almost the entire mid-low latitudes, and the M constellation had only a blank coverage in the polar region. The hybrid constellation combined the advantages of the L constellation in high latitudes and the M constellation in middle and low latitudes, with an abundance of visible satellites on a global scale, as shown in Figure 1. For the positioning scheme with only the BDS-3 system, the convergence speed of PPP improved significantly. After the introduction of the L, M, and L+M constellations, the convergence time was reduced from 45 min to 2 min, which is a 96% reduction.

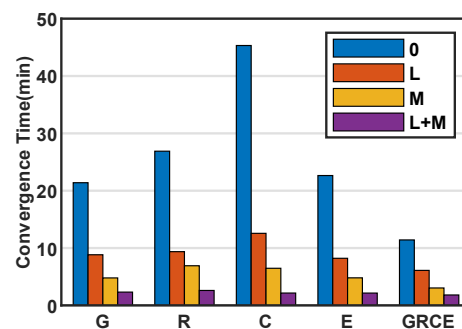


Figure 5. Comparison of average convergence times of PPP enhanced using different LEO constellations.

Figure 6 shows the average TTFF of the PPP-AR enhanced with different LEO constellations. In this study, TTFF was defined as the time required for at least five epochs to successfully achieve a fixed ambiguity solution. By introducing the L, M, and L+M constellations, the TTFF of single-system PPP could be shortened from 14.7 to 10.4, 9.4, and 7.9 min, respectively, and the time to first fix of the four-system combination PPP could be shortened from 8.6 to 6.8, 4.8, and 4.5 min, respectively. Similar to the float solution, the L+M constellation was the best, followed by the M constellation, and then the L constellation. The fixed solution showed only a 46% improvement, compared with a 92% improvement for the single-system float solution.

Table 2 shows the average positioning accuracy of different LEO constellation-augmented PPP and PPP-AR in the east, north, and up directions, respectively. Again, the reference coordinate of this study was the coordinate value in the SNX weekly solution file provided by the IGS, and the positioning accuracy was represented by the positioning error of the last epoch. The positioning accuracy of ambiguity-float solution PPP in E, N, and U

directions was 0.40, 0.34, and 1.20 cm, respectively, and that of ambiguity-fixed solution PPP was 0.28, 0.27, and 1.00 cm, respectively. With the help of the LEO constellation, the positioning accuracy of the float and fixed solutions was improved to varying degrees. The L+M constellation in the E and U directions was superior to the M and L constellations. However, the overall improvement was very limited. Even in the U-direction with the poorest positioning accuracy, the improvement was less than half a centimeter.

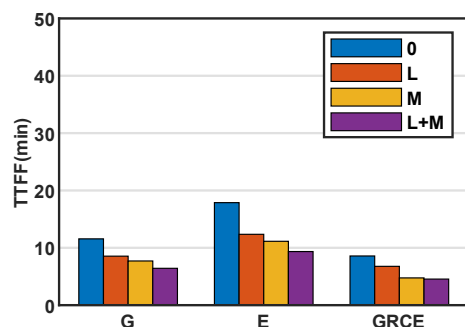


Figure 6. Comparison of average TTFF of PPP-AR, enhanced with different LEO constellations.

Table 2. Average positioning accuracy of different LEO constellations augmented PPP and PPP-AR in east (E), north (N), and up (U) directions, respectively.

Constellations	Float Solution/cm			Fixed Solution/cm		
	E	N	U	E	N	U
G	0.3560	0.2523	0.8695	0.3554	0.2549	0.8803
G+L	0.3254	0.2381	0.8139	0.3378	0.2413	0.8245
G+M	0.2390	0.2334	0.7251	0.2920	0.2366	0.7302
G+L+M	0.2130	0.2220	0.7103	0.2668	0.2239	0.7131
R	0.3214	0.3072	0.9848			
R+L	0.2938	0.2787	0.8455			
R+M	0.2727	0.3086	0.7377			
R+L+M	0.2397	0.2948	0.7233			
C	0.8484	0.5709	2.0243			
C+L	0.6016	0.3748	1.1799			
C+M	0.4335	0.4611	0.8451			
C+L+M	0.2925	0.3811	0.7211			
E	0.2628	0.2755	1.0658	0.2447	0.2740	1.0661
E+L	0.2388	0.2520	0.9140	0.2337	0.2518	0.9179
E+M	0.2374	0.2860	0.7660	0.2245	0.2810	0.7712
E+L+M	0.2150	0.2732	0.7283	0.2066	0.2703	0.7313
GRCE	0.2294	0.2844	1.0538	0.2309	0.2830	1.0593
GRCE+L	0.2173	0.2787	0.9864	0.2204	0.2781	0.9915
GRCE+M	0.2094	0.2891	0.8848	0.2118	0.2887	0.8895
GRCE+L+M	0.2020	0.2786	0.8171	0.2056	0.2777	0.8214
+0	0.4036	0.3381	1.1996	0.2770	0.2706	1.0019
+L	0.3354	0.2845	0.9479	0.2640	0.2571	0.9113
+M	0.2784	0.3156	0.7917	0.2428	0.2688	0.7970
+L+M	0.2324	0.2899	0.7400	0.2263	0.2573	0.7553

4.2.2. LEO-Enhanced PPP and PPP-AR in Different Latitudes

Considering that the enhancement of performance at different locations may vary, the 258 stations were divided into low-, middle-, and high-latitude zones for analysis. Figure 7a shows the average convergence time of PPP enhanced using the same LEO constellation at different latitudes. The average convergence time of the L constellation-enhanced PPP in low, middle, and high latitudes was 14.1, 7.8, and 3.3 min, respectively. The higher the latitude, the faster the convergence speed. This was because the polar orbital constellation was mostly at higher latitudes, so it provided more visible satellites, as shown in Figure 1a.

The average convergence time of the M constellation in the middle-latitude region was 4.6 min, which was slightly faster than the 5.4 min of the low-latitude region and the 7.0 min of the high-latitude region. This was because the M constellation provided the largest number of visible satellites in midlatitudes, as shown in Figure 1b. The average convergence times of the L+M constellation in low, middle, and high latitudes were 2.8, 2.0, and 1.9 min, respectively. The convergence speed became faster with increasing latitude. Compared with the L and M constellations, the L+M constellation presented the least significant latitude difference in the acceleration of convergence time. Figure 7b shows the average TTFF of the PPP-AR enhanced using the same LEO constellation at different latitudes. Unlike ambiguity-float solutions, the TTFF of ambiguity-fixed solution PPP enhanced using the three LEO constellations showed the same latitude difference as that of the non-LEO constellation-enhanced PPP-AR. This was because the degree of enhancement of fixed-solution PPP enhanced using LEO was weaker than that of the float solution. After the introduction of LEO satellites, it did not obviously follow that the more LEO satellites there were, the shorter the TTFF would be, as shown in Section 4.2.1.

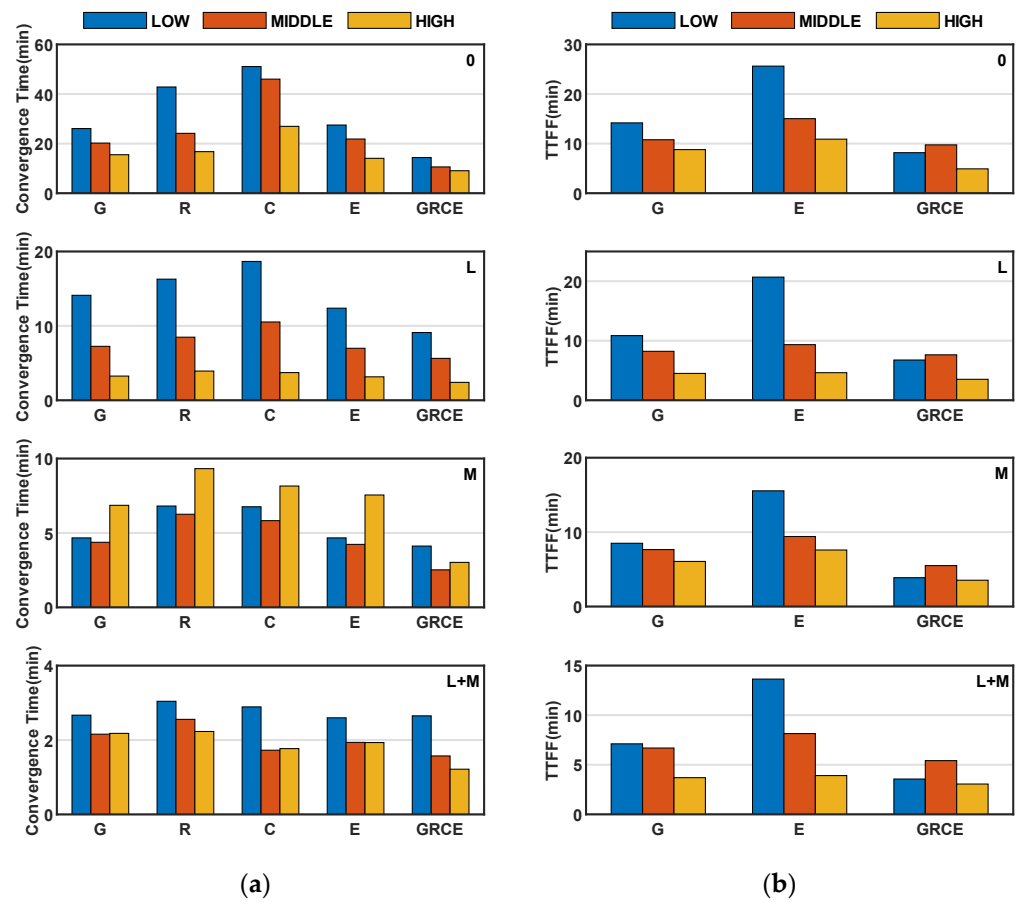


Figure 7. Comparison of convergence performance of PPP and PPP-AR enhanced using the same LEO constellation in different latitudes: (a) PPP; (b) PPP-AR.

Figure 8a,b compares the convergence performance of the PPP and the PPP-AR enhanced with different LEO constellations at the same latitude. For both the float and the fixed solutions, the L+M mixed constellation was superior to the nonmixed constellation in every latitude region. At low and middle latitudes, M was superior to L. The advantages of the L constellation were shown in the high-latitude region; compared with the float solution, the fixed-solution PPP in any latitude region had no significant enhancement difference with different LEO constellations.

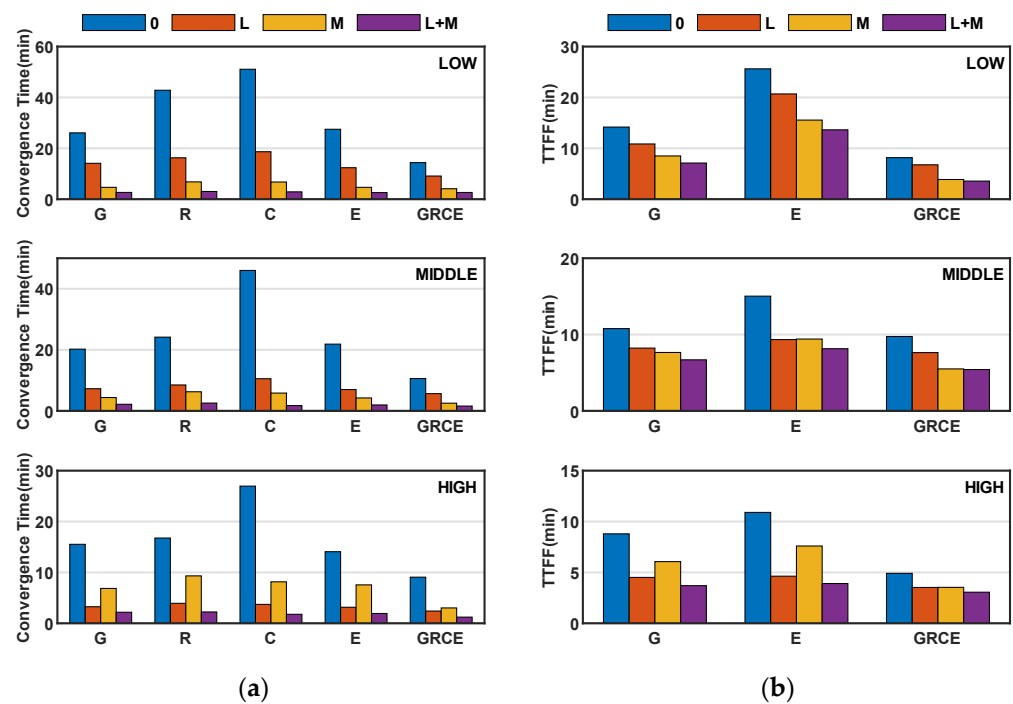


Figure 8. Comparison of convergence performance of PPP and PPP-AR enhanced with different LEO constellations in the same latitude region: (a) PPP; and (b) PPP-AR.

4.2.3. PPP and PPP-AR Enhanced by Different LEO Satellite Numbers

To further study the relationship between PPP and PPP-AR enhanced with the LEO constellation and the number of LEO satellites, we designed four experiments to control the number of LEO satellites. It should be noted that the LEO constellation used in this experiment was the L+M mixed constellation. Two LEO satellites have been taken as an example, to illustrate the method of controlling the number of LEO satellites in this study: when there were more than two LEO satellites, the first two satellites were retained according to the elevation angle. If one of the retained LEO satellites fell (i.e., the elevation angle became lower than the cutoff angle), the satellite with the higher elevation angle was selected for replacement.

Figure 9 shows the convergence times of one, two, three, four, and 'all' LEO satellites that enhanced the single-system PPP at different latitudes. One LEO satellite hardly accelerated the convergence, whereas two, three, four, and 'all' LEO satellites could accelerate the convergence time of the single-system PPP from approximately half an hour to 8.7, 4.4, 3.1, and 2.3 min, respectively. The convergence speed increased nonlinearly with the increase in the number of LEO satellites, and gradually reached saturation. Meanwhile, the latitude difference in the convergence time almost disappeared with the control of the number of LEO satellites. This also explained why the latitude difference in convergence time in Figure 7a was caused by the difference in the number of visible LEO satellites.

Figure 10 shows the TTFF of one, two, three, four, and 'all' LEO satellites with enhanced single-system PPP-AR at different latitudes. As with the float solution, one LEO satellite hardly accelerated the first fixation of ambiguity, while two, three, four, and 'all' LEO satellites accelerated the TTFF of the single-system PPP-AR from approximately 15 min to 9.0, 7.5, 6.8, and 6.4 min, respectively. However, unlike the float solution, the TTFF for the fixed-solution PPP did not decrease significantly with an increase in the number of LEO satellites, and was close to saturation when there were four LEO satellites. This also indicated that the latitude difference of the TTFF in Figure 7b was not caused by the latitude difference in the number of visible LEO satellites, but by the latitude difference of the first fixed time itself.

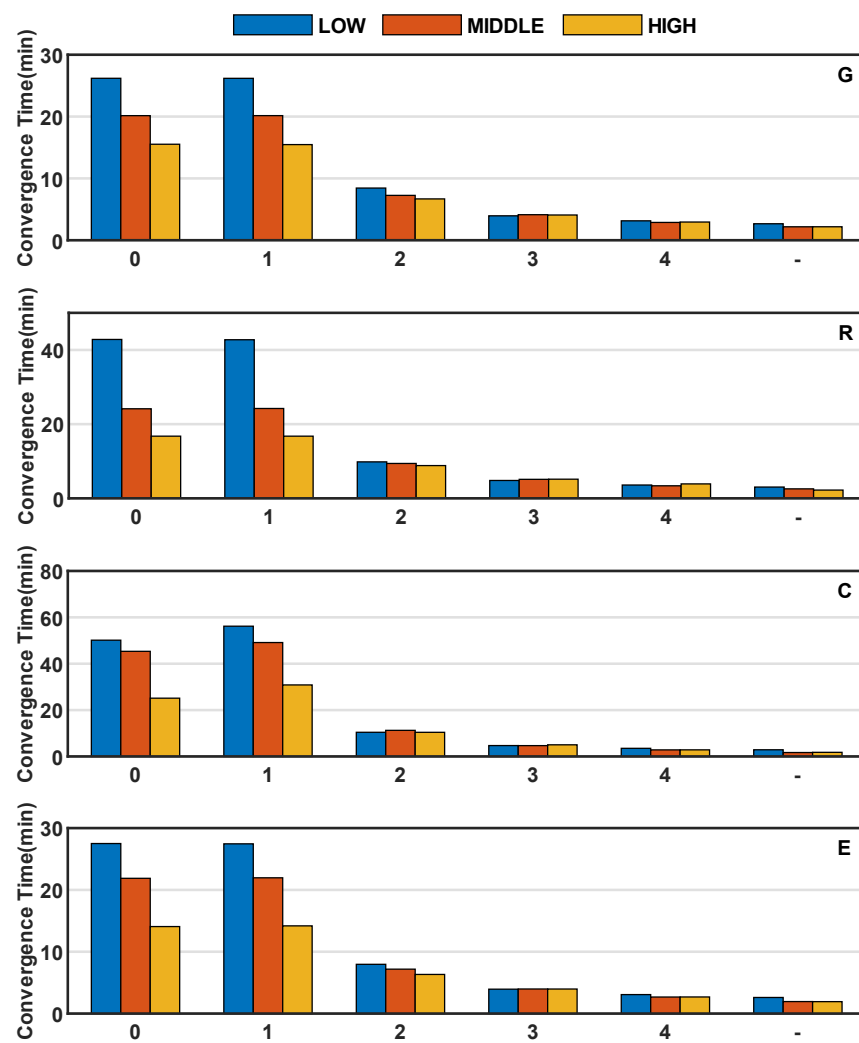


Figure 9. Comparison of convergence time of one (1), two (2), three (3), four (4), and all (-) LEO satellites enhanced single-system PPP in different latitudes.

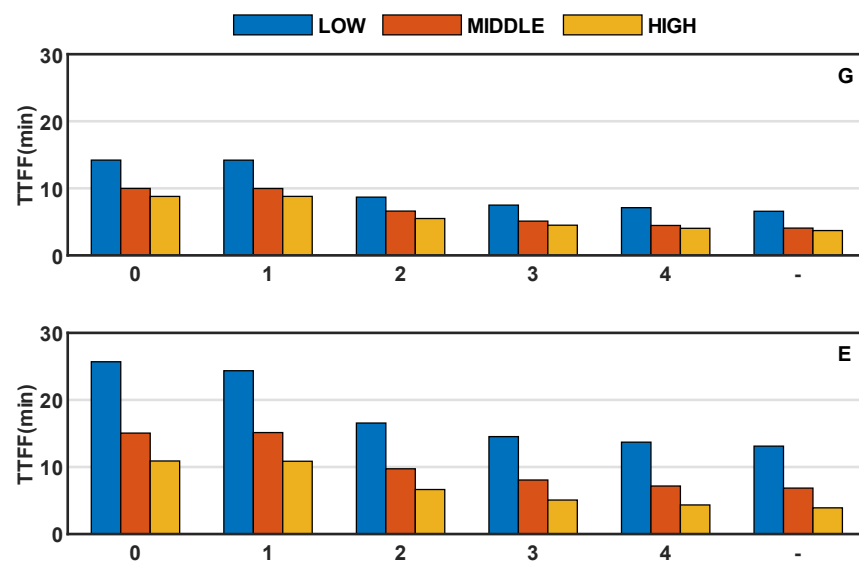


Figure 10. Comparison of TTFF of one (1), two (2), three (3), four (4), and all (-) LEO satellites enhanced single-system PPP-AR in different latitudes.

5. Conclusions and Discussion

This paper focused on the positioning performance of single-system and four-system combined PPP-AR enhanced with the LEO ambiguity-float solution, to determine if the float solution could realize PPP-AR in a shorter TTFF. We designed two LEO constellations, L and M. L was a typical polar orbit constellation, with a larger number of visible satellites at high latitudes than at low and middle latitudes. M compensated for the shortage of visible satellites in L at low and middle latitudes, but it had no coverage in the polar regions. The ground observation data of the LEO satellites at the MGEX stations were simulated. Because GNSSs were fully operational, the GNSS data were real observation data from the MGEX stations. This study evaluated the positioning performance of LEO ambiguity-float solution-enhanced PPP-AR and compared it with LEO-enhanced PPP, based on the daily observation dataset collected at 258 stations in the global MGEX observation network over three days, from 1 January to 3 January 2022, in addition to LEO simulation data.

In our estimated global GCE FCBs products, the NL FCBs of most GPS and Galileo satellites changed within 0.1 cycles in a day. For BDS-3, the stability was relatively poor. Satellites C34 and C46 had the largest changes, up to 0.6 cycles, while other satellites had changes within 0.4 cycles. The average STD of the NL FCBs for G, C, and E were 0.016, 0.054, and 0.014 cycles, respectively.

By introducing L, M, and L+M constellations, the convergence time of single-system PPP was shortened from 29.1 to 9.7, 5.7, and 2.3 min, and the TTFF was shortened from 14.7 to 10.4, 9.4, and 7.9 min, respectively. The convergence time of the four-system combination PPP was shortened from 11.4 to 6.1, 3.0, and 1.8 min, and the TTFF was shortened from 8.6 to 6.8, 4.8, and 4.5 min. The L+M mixed constellation was the best solution for shortening convergence time of PPP and TTFF, followed by the M, and then the L constellation.

Considering that the enhancement performance of the stations at different locations may vary, the 258 stations were divided into low-, middle-, and high-latitude zones for analysis. For ambiguity-float solutions, the convergence time of the L constellation-enhanced PPP in low, middle, and high latitudes was 14.1, 7.8, and 3.3 min, respectively. The higher the latitude, the faster the convergence speed. The convergence time of the M constellation-enhanced PPP in low, middle, and high latitudes was 5.4, 4.6, and 7.0 min, respectively. The convergence time of the L+M mixed constellations in low, middle, and high latitudes was within 3 min, and the latitude difference was not significant. Unlike ambiguity-float solutions, for the TTFF, the ambiguity-fixed solution PPP enhanced using the three LEO constellations showed the same latitude difference as that of the non-LEO constellation-enhanced PPP-AR.

To further study the relationship between both PPP and PPP-AR enhanced with the LEO constellation and the number of LEO satellites, we controlled the number of LEO satellites in the L+M mixed constellation. For ambiguity-float solutions, the convergence speed increased nonlinearly with an increase in the number of LEO satellites, and gradually reached saturation. Meanwhile, the latitude difference in the convergence time almost disappeared with the control of the number of LEO satellites. For fixed-solution PPP, the TTFF decreased with an increase in the number of LEO satellites (which was not significant) and was close to saturation for four LEO satellites.

We recommend the use of a mixed low-orbit constellation that integrates both inclined orbit satellites and polar orbit satellites, which have good enhancement performance not only in high latitudes but, more importantly, in low and middle latitudes as well. Since the world population is mostly distributed in the middle and low latitudes, the shorter convergence time in this region is more meaningful than that it would be in the high latitudes. In addition, the LEO float solution was employed to enhance PPP-AR. This method was undoubtedly a better choice when the ground tracking network of the LEO system was not perfect enough to solve the LEO FCB to fix the LEO satellite ambiguity, which can reduce the time to first fix of the four-system combined PPP-AR to 5 min on the global scale (thus reducing the contingency caused by selecting typical examples). In addition, it does not require too many LEO satellites; four is enough. Similarly,

Hong et al. [36] also used this method to study the rapid precise point positioning enhanced with low Earth orbit satellites, pointing out that (based on the small-scale European stations) the time to first fix using the G single system as well as the G/C/E combined system with LEO satellites added could be reduced by 86.4% and 82.8%, respectively, with respect to systems without additional LEO satellites.

Author Contributions: Q.L., W.Y. and R.T. provided the initial idea for this work and wrote this manuscript; Q.L. designed the algorithm; Q.L., W.Y., R.T., Y.D. and M.L. contributed to the analyses of results; Q.L. and R.T. drew the pictures. All authors have read and agreed to the published version of the manuscript.

Funding: This research was funded by the National Natural Science Foundation of China, grant number 41974032, 42274019.

Data Availability Statement: The raw/processed data required to reproduce these findings cannot be shared at this time as the data also forms part of an ongoing study.

Acknowledgments: The work was supported by the Chinese Academy of Sciences (CAS) programs of “High Level Talents”.

Conflicts of Interest: The authors declare no conflict of interest.

References

- Zumberge, J.F.; Heflin, M.B.; Jefferson, D.C.; Watkins, M.M.; Webb, F.H. Precise point positioning for the efficient and robust analysis of GPS data from large networks. *J. Geophys. Res. Solid Earth* **1997**, *102*, 5005–5017. [\[CrossRef\]](#)
- Chen, L.; Zheng, F.; Gong, X.; Jiang, X. GNSS High-Precision Augmentation for Autonomous Vehicles: Requirements, Solution, and Technical Challenges. *Remote Sens.* **2023**, *15*, 1623. [\[CrossRef\]](#)
- Gabor, M.J.; Nerem, R.S. GPS carrier phase AR using satellite-satellite single difference. In Proceedings of the 12th International Technical Meeting of the Satellite Division of the Institute of Navigation (GPS 99), Nashville, TN, USA, 14–17 September 1999.
- Ge, M.; Gendt, G.; Rothacher, M.; Shi, C.; Liu, J. Resolution of GPS carrier phase ambiguities in precise point positioning (PPP) with daily observations. *J. Geod.* **2008**, *82*, 389–399. [\[CrossRef\]](#)
- Wübbena, G.; Schmitz, M.; Bagge, A. PPP-RTK: Precise point positioning using state-space representation in RTK networks. In Proceedings of the 18th International Technical Meeting of the Satellite Division of The Institute of Navigation (ION GNSS 2005), Long Beach, CA, USA, 13–16 September 2005; pp. 2584–2594.
- Teunissen, P.J.G.; Khodabandeh, A. Review and principles of PPP-RTK methods. *J. Geod.* **2015**, *89*, 217–240. [\[CrossRef\]](#)
- Cai, C. *Precise Point Positioning Using Dual-Frequency GPS and GLONASS Measurements*; University of Calgary: Calgary, AB, Canada, 2009.
- Tolman, B.W.; Kerkhoff, A.; Rainwater, D.; Munton, D.; Banks, J. Absolute precise kinematic positioning with GPS and GLONASS. In Proceedings of the 23th International Technical Meeting of the Satellite Division of The Institute of Navigation (ION GNSS 2010), 21–24 September 2010; pp. 2565–2576.
- Jokinen, A.; Feng, S.; Schuster, W.; Ochieng, W.; Hide, C.; Moore, T.; Hill, C. GLONASS Aided GPS Ambiguity Fixed Precise Point Positioning. *J. Navig.* **2013**, *66*, 399–416. [\[CrossRef\]](#)
- Li, P.; Zhang, X. Integrating GPS and GLONASS to accelerate convergence and initialization times of precise point positioning. *GPS Solut.* **2014**, *18*, 461–471. [\[CrossRef\]](#)
- Tegedor, J.; Øvstedal, O.; Vigen, E. Precise orbit determination and point positioning using GPS, Glonass, Galileo and BeiDou. *J. Geod. Sci.* **2014**, *4*, 65–73. [\[CrossRef\]](#)
- Li, X.; Ge, M.; Dai, X.; Ren, X.; Fritsche, M.; Wickert, J.; Schuh, H. Accuracy and reliability of multi-GNSS real-time precise positioning: GPS, GLONASS, BeiDou, and Galileo. *J. Geod.* **2015**, *89*, 607–635. [\[CrossRef\]](#)
- Li, X.; Li, X.; Yuan, Y.; Zhang, K.; Zhang, X.; Wickert, J. Multi-GNSS phase delay estimation and PPP ambiguity resolution: GPS, BDS, GLONASS, Galileo. *J. Geod.* **2018**, *92*, 579–608. [\[CrossRef\]](#)
- Geng, J.; Bock, Y. Triple-frequency GPS precise point positioning with rapid ambiguity resolution. *J. Geod.* **2013**, *87*, 449–460. [\[CrossRef\]](#)
- Mohamed, E. Precise Point Positioning using Triple-Frequency GPS Measurements. *J. Navig.* **2014**, *68*, 480–492.
- Li, P.; Zhang, X.; Ge, M.; Schuh, H. Three-frequency BDS precise point positioning ambiguity resolution based on raw observables. *J. Geod.* **2018**, *92*, 1357–1369. [\[CrossRef\]](#)
- Li, X.; Li, X.; Liu, G.; Feng, G.; Yuan, Y.; Zhang, K.; Ren, X. Triple-frequency PPP ambiguity resolution with multi-constellation GNSS: BDS and Galileo. *J. Geod.* **2019**, *93*, 1105–1122. [\[CrossRef\]](#)
- Banville, S.; Collins, P.; Zhang, W.B.; Langley, R. Global and Regional Ionospheric Corrections for Faster PPP Convergence. *Navigation* **2014**, *61*, 115–124. [\[CrossRef\]](#)

19. Psychas, D.; Verhagen, S. Real-Time PPP-RTK Performance Analysis Using Ionospheric Corrections from Multi-Scale Network Configurations. *Sensors* **2020**, *20*, 3012. [[CrossRef](#)]
20. Reid, T.G.; Neish, A.M.; Walter, T.F.; Enge, P.K. Leveraging Commercial Broadband LEO Constellations for Navigation. In Proceedings of the 29th International Technical Meeting of the Satellite Division of The Institute of Navigation (ION GNSS 2016), Portland, OR, USA, 12–16 September 2016; pp. 2300–2314.
21. Enge, P.; Ferrell, B.; Bennet, J.; Whelan, D.; Gutt, G.; Lawrence, D. Orbital Diversity for Satellite Navigation. In Proceedings of the 25th International Technical Meeting of the Satellite Division of The Institute of Navigation (ION GNSS 2012), Nashville, TN, USA, 17–21 September 2012; pp. 3834–3846.
22. Li, M.; Xu, T.; Guan, M.; Gao, F. LEO-constellation-augmented multi-GNSS real-time PPP for rapid re-convergence in harsh environments. *GPS Solut.* **2022**, *26*, 29. [[CrossRef](#)]
23. Ke, M.; Lv, J.; Chang, J.; Dai, W.; Tong, K.; Zhu, M. Integrating GPS and LEO to accelerate convergence time of precise point positioning. In Proceedings of the 7th International Conference on Wireless Communications and Signal Proceeding (WCSP), Nanjing, China, 15–17 October 2015; pp. 1–5.
24. Ge, H.; Li, B.; Ge, M.; Zang, N.; Nie, L.; Shen, Y.; Schuh, H. Initial Assessment of Precise Point Positioning with LEO Enhanced Global Navigation Satellite Systems (LeGNSS). *Remote Sens.* **2018**, *10*, 984. [[CrossRef](#)]
25. Li, X.; Ma, F.; Li, X.; Lu, H.; Blan, L.; Jiang, Z.; Zhang, X. LEO constellation-augmented multi-GNSS for rapid PPP convergence. *J. Geod.* **2018**, *93*, 749–764. [[CrossRef](#)]
26. Li, X.; Li, X.; Ma, F.; Yuan, Y. Improved PPP ambiguity resolution with the assistance of multiple LEO constellations and signals. *Remote Sens.* **2019**, *11*, 408. [[CrossRef](#)]
27. Zhao, Q.; Pan, S.; Gao, C. BDS/GPS/LEO triple-frequency uncombined precise point positioning and its performance in harsh environments. *Measurement* **2020**, *151*, 107216. [[CrossRef](#)]
28. Walker, J.G. Satellite constellations. *J. Br. Interplanet. Soc.* **1984**, *37*, 559–572.
29. Saastamoinen, J. Atmospheric correction for the troposphere and stratosphere in radio ranging satellites. *Use Artif. Satell. Geod.* **1972**, *15*, 247–251.
30. Böhm, J.; Niell, A.; Tregoning, P.; Schuh, H. Global Mapping Function (GMF): A new empirical mapping function based on numerical weather model data. *Geophys. Res. Lett.* **2006**, *33*, 1–4. [[CrossRef](#)]
31. Kouba, J. A Guide to Using International GNSS Service (IGS) Products. 2009. Available online: <http://igsceb.jpl.nasa.gov/igsceb/resource/pubs/UsingIGSProductsVer21.pdf> (accessed on 15 January 2019).
32. King, R.W. *Documentation for the GAMIT GPS Analysis Software*; Massachusetts Institute of Technology: Cambridge, MA, USA, 1995.
33. Hatch, R. The synergism of GPS code and carrier measurements. In Proceedings of the 3rd International Symposium on Satellite Doppler Positioning at Physical Sciences Laboratory of New Mexico State University, Las Cruces, NM, USA, 8–12 February 1982; pp. 1213–1231.
34. Melbourne, W.G. The case for ranging in GPS-based geodetic systems. In Proceedings of the 1st International Symposium on Precise Positioning with the Global Positioning System, Rockville, MD, USA, 15–19 April 1985; pp. 373–386.
35. Wübbena, G. Software developments for geodetic positioning with GPS using TI 4100 code and carrier measurements. In Proceedings of the 1st International Symposium on Precise Positioning with the Global Positioning System, Rockville, MD, USA, 15–19 April 1985; pp. 403–412.
36. Hong, J.; Tu, R.; Zhang, P.; Zhang, R.; Fan, L.; Wang, S.; Lu, X. GNSS rapid precise point positioning enhanced by low Earth orbit satellites. *Satell. Navig.* **2023**, *4*, 11. [[CrossRef](#)]

Disclaimer/Publisher’s Note: The statements, opinions and data contained in all publications are solely those of the individual author(s) and contributor(s) and not of MDPI and/or the editor(s). MDPI and/or the editor(s) disclaim responsibility for any injury to people or property resulting from any ideas, methods, instructions or products referred to in the content.